Inorganic Chemistry

Article

pubs.acs.org/IC

Corrole-BODIPY Dyads: Synthesis, Structure, and Electrochemical and Photophysical Properties

Biju Basumatary, Adiki Raja Sekhar, R. V. Ramana Reddy, and Jeyaraman Sankar*

Department of Chemistry, Indian Institute of Science Education and Research Bhopal, Indore Bypass Road, Bhopal, India 462066

Supporting Information

ABSTRACT: A free-base and its Cu(III) derivative of bichromophoric meso-β linked corrole-BODIPY dyad were synthesized and structurally characterized by single crystal X-ray diffraction (XRD). Both corrole and BODIPY fragments maintained respective ground state electronic isolation despite their connection through a single bond due to a tilted orientation as observed by XRD. This was further supported by UV−vis and cyclic voltammetric studies. The Cu(III)-metalated dyad exhibits temperature-dependent paramagnetic behavior as observed in the variable temperature ^{1}H NMR due to the presence of a Cu(II)-corrole-π-cation radical. Importantly, the free-base exhibits complete fluorescence quenching probably due to photoinduced electron transfer to a low lying charge separated state. Interestingly, emission was regained upon addition of 1,8-diazabicyclo[5.4.0]undec-7-ene (DBU) due to the deprotonation of corrole. The "turn on" fluorescence behavior and the presence of acidic NH protons were further exploited toward basic anion sensing utility.

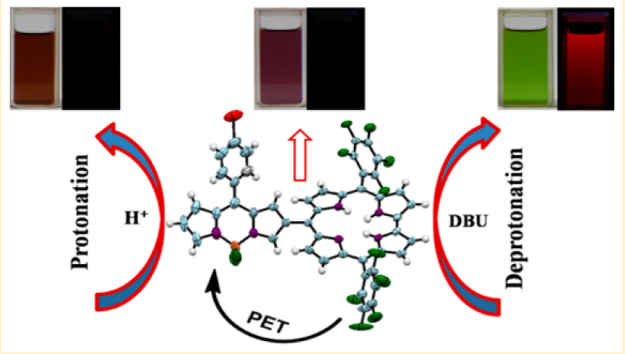

1. INTRODUCTION

Corroles are tetrapyrrolic, 18 π-electron Hückel aromatic macrocycles closely related to porphyrin with a direct pyrrole−pyrrole linkage lacking one methine bridge. The first synthesis of corrole was carried out by Johnson and Kay[1] in the late 1960s, motivated because of the similarity of corroles to that of cobalt chelating corrin in vitamin B_{12}. A one-pot synthesis pioneered by Gross et al. in 1999 followed by remarkable development in the synthesis of corrole[2−6] revolutionized the understanding of this unique tetrapyrrolic ligand.

Corrole shows a relatively higher fluorescence quantum yield and molar absorptivity than corresponding porphyrin macrocycles.[7] Moreover, the noninnocent nature of the corrole ligand[8] in many metallo-complexes is now well documented. The trianionic nature due to three inner nitrogen protons imparts many intriguing properties to corroles which are significantly different from that of porphyrin macrocycles. Its ability to stabilize relatively higher oxidation states of metal than those of the corresponding porphyrin complexes augmented the exploration of many metallocorroles in oxidative catalysis,[9] group transfer catalysis,[10] and reduction catalysis.[11] Apart from this, corrole has demonstrated potential applications in the field of photochemical sensors,[12] artificial photosynthesis,[13] and biomedical applications[14] during the last two decades.

Free-base corroles show less stability against light and air than the porphyrin macrocycles. Lower stability mainly originates from the electron-rich nature of corrole, reduced aromaticity, and deformation of the macrocycles from planarity due to steric hindrance at the core. Thus, the free-base 5,10,15-tris(pentafluorophenyl)corrole [H_3(tpfc)] has been identified to be stable under oxidative degradation in light and air due to the presence of electron withdrawing pentafluorophenyl groups at the meso-carbon and probably a choice where higher stability is desired.[15] Both synthetic and stability constraints limited further functionalization of corroles readily. Nevertheless, a few successful functionalizations of corrole reported in the literature shows a significant effect on the electronic properties of corrole.[16] Functionalization of aryl ring at the meso-position and on the β-pyrrolic position is the most common and relatively easy way of modification. Therefore, partly inspired by the lack of literature reports on chromophoric functionalization at the meso-carbon of corrole and to understand the electronic effect of this unique connectivity, we report here the first successful direct meso-β linked corrole-BODIPY conjugates. The structures and electronic and optical properties of these functionalized bi-chromophoric novel dyads were investigated, and furthermore their unique fluorescence turn on behavior was explored toward an anion sensing ability.

2. EXPERIMENTAL SECTION

2.1. General Consideration. Pentafluorobenzaldehyde, 2,3-dichloro-5,6-dicyanobenzoquinone (DDQ), trifluoroacetic acid (TFA), and tetrabutylammonium hexafluorophosphate (TBAPF)

Received: December 9, 2014
Published: April 15, 2015

DOI: 10.1021/ic502919s
Inorg. Chem. 2015, 54, 4257−4267

were purchased from Sigma-Aldrich. 4-Bromobenzldehyde, triethylamine (Et_3N), pyrrole, phosphorus oxychloride ($POCl_3$), and $Cu(OAc)_2·H_2O$ were purchased from Merck and Spectrochem, India. Other chemicals were of reagent grade. Hexane, DMF, $POCl_3$, CH_2Cl_2, $CHCl_3$, and ethyl acetate were distilled according to standard procedures prior to use. HPLC-grade solvents were used for spectroscopy and electrochemical studies.

2.2. Instrumentation. ^1H, ^{13}C, ^{19}F, and ^{11}B NMR spectra were recorded on Bruker 400, 500, and 700 MHz instruments using $CDCl_3$ as a solvent. Chemical shifts were given in parts per million relative to residual $CHCl_3$ (7.240 ppm). Two-dimensional (2D) NMR experiments were performed on a Bruker 400 or 500 MHz instrument. UV−vis absorption experiments were performed on an Agilent Cary-100 with 1 cm path length quartz cuvette, and fluorescence emission spectra were recorded on a Horiba Fluorolog spectrophotometer. High resolution mass spectroscopy (HRMS) electrospray ionization (ESI) mass spectra and atmospheric pressure chemical ionization (APCI) mass spectra were recorded on a Bruker micro TOF-Q II mass spectrometer. Matrix assisted laser desorption/ionization (MALDI) were recorded on a Bruker ultra flextreme mass spectrometer. Cyclic voltammograms were carried out using a three-electrode system consisting of a Pt disk as working electrode, Ag/Ag^+ reference electrode, and a Pt-wire as counter electrode on a CH-Instrument potentiostat. Tetrabutylammonium hexafluorophosphate (TBAPF) in dichloromethane was used as supporting electrolyte (0.1 M). X-ray diffraction measurements were carried out at 300 K (**2** and **3**) and 105 K (**6**), on a Bruker APEX II diffractometer equipped with a graphite monochromator and Mo Kα (λ = 0.71073 Å) radiation. Data collections were performed using ϕ and ω scans. The structures were solved using direct methods followed by full matrix least-squares refinements against F^2 (all data HKLF 4 format) using SHELXTL. All refinements were carried out using SHELXL 97, PLATON 99, and WinGX systemVer-1.6414. Disordered solvent molecules were removed by using SQUEEZE command in PLATON. All computational investigations were performed with the Gaussian 09 program. For computational studies, initial geometry for compound **6** was taken from single crystal data and fully optimized without any symmetry restriction. The calculations were performed by the density functional theory (DFT) method with restricted B3LYP (Becke's three-parameter hybrid exchange functional and Lee−Yang−Parr correlation function) level, employing basis sets 6-31G(d) for H, B, C, N, F, and Br and LANL2DZ for Cu.

2.3. Synthesis and Characterization of Compounds. *4-Bromophenyl BODIPY (**2**).* BODIPY **2** was prepared in a one-pot, two-step synthetic procedure according to the modified literature method.[17] DDQ (227 mg, 1 mmol) in $CHCl_3$ (10 mL) was added to **1** (301 mg, 1 mmol) in 50 mL of $CHCl_3$, cooled in an ice bath under N_2 atmosphere. The reaction mixture was stirred for 10 min. Triethylamine (2 mL) and immediately followed by $BF_3·Et_2O$ (2 mL) were added to the reaction mixture. The reaction mixture was further stirred for another 3 h at room temperature and washed with 0.2 M NaOH solution (100 mL) and water (100 mL). The organic layer was collected and dried over anhydrous Na_2SO_4, and the solvent was removed under reduced pressure. The crude product was purified by using silica gel column chromatography (100−200 mesh) using ethyl acetate/hexane (10:90, v/v) as an eluent to give the desired product and characterized. Yield = 72% (250 mg, 0.72 mmol), reddish crystalline solid. UV−vis (CH_2Cl_2): λ_{max}, nm ($\varepsilon \times 10^{-4}$, M^{-1} cm^{-1}); 352 (1.88), 503 (6.3). ^1H NMR (400 MHz; $CDCl_3$; 298 K): δ 6.54 (d, $^3J_{H-H}$ = 4.1 Hz, 2H, *pyrrolic*), δ 6.89 (d, $^3J_{H-H}$ = 4.2 Hz, 2H, *pyrrolic*), δ 7.43 (d, $^3J_{H-H}$ = 8.5, 2H, *Ph*), δ 7.67 (d, $^3J_{H-H}$ = 8.5, 2H, Ph), δ 7.94 (s, 2H, *pyrrolic*). ^{13}C NMR (101 MHz; $CDCl_3$; 298 K): δ 118.76, 125.42, 131.29, 131.81, 132.57, 134.64, 144.54, 145.73. ^{19}F NMR (376 MHz; $CDCl_3$; 298 K): δ −145.08 (dd, $^1J_{F-B}$ = 57.5 Hz, $^1J_{F-B}$ = 28.7, 2F, BF_2), ^{11}B NMR (128 MHz; $CDCl_3$; 298 K): δ 0.25 (t, $^1J_{B-F}$ = 28.7 Hz, 1B, BF_2). HR-MS (APCI): Calculated for $C_{15}H_{10}BBrF_2N_2$ [$(M)^+$]: 346.0086, observed: 346.0098

*β-Formyl BODIPY (**3**).* Freshly distilled $POCl_3$ (10 mL) was slowly added to DMF (10 mL), cooled in an ice bath under argon atmosphere, and stirred for 10 min. After being warmed to room temperature, the Vilsmeier complex was further stirred for 30 min. Compound **2** (347 mg, 1 mmol) in 1,2-dichloroethane (80 mL) was added to the reaction mixture. After the temperature was increased to 70 °C, the reaction mixture was further stirred for 12 h, cooled to room temperature, and added dropwise into a saturated aqueous solution of K_2CO_3 (500 mL) cooled in an ice bath with continuous stirring. After being warmed to room temperature, the reaction mixture was further stirred for 1 h and extracted with CH_2Cl_2. The organic layers were combined, washed with water, and dried over anhydrous $NaSO_4$, and the solvent was removed under reduced pressure. The crude product was purified by silica gel column chromatography (100−200 mesh) using ethyl acetate/hexane (20:80, v/v) as an eluent to give desired product and characterized. Yield = 65% (263 mg, 0.65 mmol), reddish-brown crystalline solid. UV−vis (CH_2Cl_2): λ_{max}, nm ($\varepsilon \times 10^{-4}$, M^{-1} cm^{-1}) 365 (2.05), 499 (7.65). ^1H NMR (400 MHz; $CDCl_3$; 298 K): δ 6.72 (d, $^3J_{H-H}$ = 4.5 Hz, 1H, *pyrrolic*), δ 7.10 (d, $^3J_{H-H}$ = 4.5 Hz, 1H, *pyrrolic*), δ 7.25 (s, 1H, *pyrrolic*), δ 7.44 (d, $^3J_{H-H}$ = 8.5, 2H, *Ph*), δ 7.71 (d, $^3J_{H-H}$ = 8.5 Hz, 2H, *Ph*), δ 8.17 (s, 1H, *pyrrolic*), δ 8.26 (s, 1H, *pyrrolic*), δ 9.83 (s, 1H, *CHO*). ^{13}C NMR (101 MHz; $CDCl_3$; 298 K): δ 121.79, 126.53, 128.51, 131.71, 131.85, 131.97, 132.24, 134.26, 134.60, 136.75, 143.19, 147.96, 149.93, 184.64. ^{19}F NMR (376 MHz; $CDCl_3$, 298 K: δ −144.90 (dd, $^1J_{F-B}$ = 55.8 Hz, $^1J_{F-B}$ = 27.9 Hz, BF_2), ^{11}B NMR (128 MHz; $CDCl_3$; 298 K: δ 0.14 (t, $^1J_{B-F}$ = 27.9 Hz, 1B, BF_2). HR-MS (APCI): Calculated for $C_{16}H_{11}BBrF_2N_2O$ [$(M + H)^+$]: 375.0113, observed: m/z 375.0128

*BODIPY Dipyrromethane (**4**).* BODIPY **3** (100 mg, 0.2 mmol) and excess of freshly distilled pyrrole (0.5 mL) were added to it in a round-bottom flask under Argon atmosphere. A catalytic amount of TFA (0.1 equiv) was added to the reaction mixture and stirred vigorously for 5 min. The reaction mixture was diluted with 100 mL of CH_2Cl_2. Triethylamine (0.2 equiv) was added and stirred for another 5 min. The solvent and excess pyrrole were evaporated under reduced pressure, and the crude mixture was purified by silica gel column chromatography (100−200 mesh) using ethyl acetate/hexane (15:75, v/v) as an eluent to give the desired product, and characterized. Yield = 76% (99 mg, 0.20 mmol), red powder. ^1H NMR (400 MHz; $CDCl_3$; 298 K): δ 5.35 (s, 1H), δ 5.95 (br s, 2H), δ 6.12 (dd, $^3J_{H-H}$ = 5.7 Hz, $^4J_{H-H}$ = 2.8 Hz, 2H), δ 6.53 (dd,$^3J_{H-H}$ = 3.9 Hz, $^4J_{H-H}$ = 1.4 Hz, 1H), δ 6.64 (dd, $^3J_{H-H}$ = 3.4 Hz, $^4J_{H-H}$ = 1.4 Hz, 2H), δ 6.71 (s, 1H), δ 6.86 (d, $^3J_{H-H}$ = 4.0 Hz, 1H), δ 7.38 (d, $^3J_{H-H}$ = 8.4 Hz, 2H), δ 7.63 (d, $^3J_{H-H}$ = 8.4 Hz, 2H), δ 7.73 (s, 1H), δ 7.89 (s, 1H), δ 7.93 (s, 2H). ^{19}F NMR (376 MHz; $CDCl_3$; 298 K): δ −144.66 (dd, $^1J_{F-B}$ = 57.6 Hz, $^1J_{F-B}$ = 28.7 Hz, 2F), ^{11}B NMR (128 MHz; $CDCl_3$; 298 K: δ 0.14 (t, $^1J_{B-F}$ = 28.8, 1B). ^{13}C NMR (101 MHz; $CDCl_3$; 298 K): δ 106.97, 108.58, 117.78, 118.74, 125.64, 128.25, 128.94, 129.06, 131.24, 131.82, 131.89, 132.50, 134.58, 134.73, 135.84, 144.28, 144.45, 145.50; HR-MS (APCI): Calculated for $C_{24}H_{17}BBrF_2N_4$ [$(M - H)^+$]: 489.0696, observed: m/z 489.0653

*Corrole-BODIPY Dyad (**6**).* **3** (100 mg, 0.26 mmol) and **5** (163 mg, 0.52 mmol) were dissolved in MeOH (40 mL). A solution of HCl (aq) (36%), 1 mL in 20 mL of H_2O, was added slowly to the reaction mixture, and stirred for 2 h. The pink color reaction mixture was extracted with $CHCl_3$, and the organic layer was washed twice with H_2O, dried over anhydrous Na_2SO_4, filtered, and diluted to 100 mL with $CHCl_3$. DDQ (340 mg, 1.5 mmol) was added, and a dark green mixture was stirred for another 2 h. The reaction mixture was concentrated and subjected to filtration column through neutral alumina using CH_2Cl_2; all fractions containing product were collected and evaporated to dryness. Silica gel column chromatography (100−200 mesh) using ethyl acetate/hexane (10:90, v/v) as an eluent and repeated precipitation with hexane/methanol gave the desired product. Yield = 14% (36 mg, 0.037 mmol), purple colored powder. UV−vis (CH_2Cl_2): λ_{max}, nm ($\varepsilon \times 10^{-4}$, M^{-1} cm^{-1}) 411 (22.33), 487 (10.48), 553 (6.4), 616 (3.57). ^1H NMR (400 MHz; $CDCl_3$; 298 K): δ 6.70 (d, $^3J_{H-H}$ = 2.9 Hz, 1H, *bodipy pyrrolic*), δ 7.08 (d, $^3J_{H-H}$ = 4.0 Hz, 1H, *bodipy pyrrolic*), δ 7.63 (s, 1H, *bodipy pyrrolic*), δ 7.77−7.66 (m, 4H, *Ph*), δ 8.11 (s, 1H, *bodipy pyrrolic*), δ 8.55 (d, $^3J_{H-H}$ = 3.9 Hz, 2H, *corrole pyrrolic*), δ 8.72 (s, 1H, *bodipy pyrrolic*), δ 8.73 (d, $^3J_{H-H}$ = 5.11

DOI: 10.1021/ic502919s
Inorg. Chem. 2015, 54, 4257−4267

Scheme 1. Synthesis of Precursors 2, 3, and 4[a]

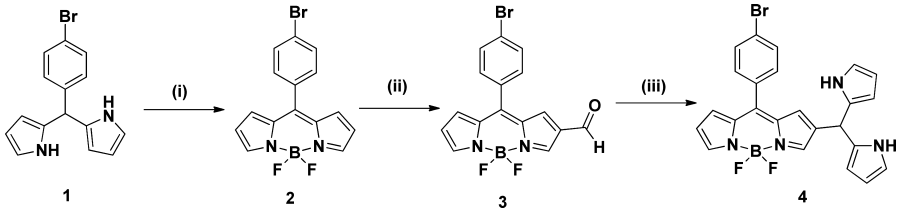

[a](i) DDQ/CH_2Cl_2, $Et_3N/BF_3{\cdot}OEt_2$, RT, 2 h, yield = 72%. (ii) DMF/$POCl_3$ at 0 °C, $C_2H_4Cl_2$, 70 °C, yield = 65%. (iii) pyrrole/TFA, RT, 4-5 min, yield = 76%.

Scheme 2. Synthesis of Compounds 6 and 7[a]

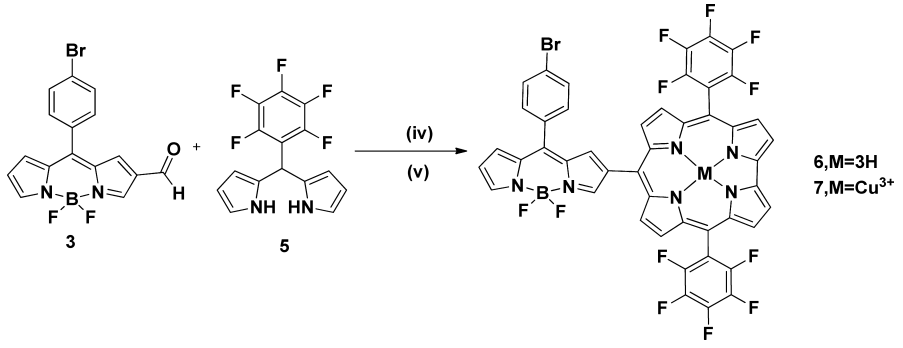

[a](iv) TFA/CH_2Cl_2, yield = 16% or $BF_3.OEt_2/CHCl_3$, DDQ, yield = 24% or MeOH/H_2O, $CHCl_3$/DDQ, yield = 14%. (v) $Cu(OAc)_2{\cdot}H_2O$, $CHCl_3$/MeOH, yield = 82%.

Hz, 2H, *corrole pyrrolic*), δ 8.91 (d, $^3J_{H-H}$ = 4.7 Hz, 2H, *corrole pyrrolic*), δ 9.08 (d, $^3J_{H-H}$ = 4.2 Hz, 2H, *corrole pyrrolic*). ^{19}F NMR (376 MHz; $CDCl_3$; 298 K: δ −160.76 (m, 4F, *meta Ph-F*), δ −152.17 (t, $^3J_{F-F}$ = 20.9 Hz, 2F, *para Ph-F*), δ −144.87 (dd, $^1J_{F-B}$ = 56.6 Hz, $^1J_{F-B}$ = 28.1 Hz, 2F, *BF*$_2$), δ −136.96 (d, $^3J_{F-B}$ = 18.8 Hz, 4F, *ortho Ph-F*). ^{11}B NMR (128 MHz; $CDCl_3$; 298 K): δ 0.26 (t, $^1J_{B-F}$ = 28.2 Hz, 1B, *BF*$_2$). HR-MS (APCI): Calculated for $C_{46}H_{21}BBrF_{12}N_6$ [(M + H)$^+$]: 975.0915, observed: *m*/*z* 975.0912

Cu(III)-corrole BODIPY Dyad (7). Compound **6** (50 mg, 0.048 mmol) was dissolved in 15 mL of $CHCl_3$/MeOH (1:2) at room temperature, and $Cu(OAc)_2{\cdot}H_2O$ (95 mg, 0.48 mmol) was added to it. The mixture was stirred for 1 h, solvent was removed under reduced pressure, and the product was purified by silica gel column chromatography (100−200 mesh) with CH_2Cl_2/hexane (2:1, v/v) as an eluent and characterized. Yield = 82%, (44 mg, 0.041 mmol), purple colored powder. UV−vis (CH_2Cl_2): λ_{max}, nm ($\varepsilon \times 10^{-4}$, M^{-1} cm^{-1}) 400 (27.11), 484 (12.13), 551 (14.00). ^{1}H NMR (700 MHz; $CDCl_3$; 298 K): δ 6.65 (d, $^3J_{H-H}$ = 3.2 Hz, 1H, *bodipy pyrrolic*), δ 7.02 (d, $^3J_{H-H}$ = 3.8 Hz, 1H, *bodipy pyrrolic*), δ 7.15 (s, 1H, *bodipy pyrrolic*), δ 7.24 (br, 2H, *corrole pyrrolic*), δ 7.44 (d, $^3J_{H-H}$ = 3.6 Hz, 2H, *corrole pyrrolic*), δ 7.50 (d, $^3J_{H-H}$ = 8.20 Hz, 2H, *ph*), δ 7.51 (d, $^3J_{H-H}$ = 4.21 Hz, 2H, *corrole pyrrolic*), δ 7.69 (d, $^3J_{H-H}$ = 8.2 Hz, 2H, *ph*), δ 7.90 (d, $^3J_{H-H}$ = 2.5 Hz, 2H, *corrole pyrrolic*), δ 8.07 (s, 1H, *bodipy pyrrolic*), δ 8.23 (s, 1H, *bodipy pyrrolic*). ^{19}F NMR (376 MHz; $CDCl_3$; 298 K): δ −160.73 (m, 4F, *meta Ph-F*), δ −152.16 (t, $^3J_{F-F}$ = 20.9 Hz, 2F, *para Ph-F*), δ −144.88 (dd, $^1J_{F-B}$ = 56.6 Hz, $^1J_{F-B}$ = 28.3 Hz, 2F, *BF*$_2$), δ −136.97 (d, $^3J_{F-B}$ = 17.8 Hz, 4F, *ortho Ph-F*). ^{11}B NMR (128 MHz; $CDCl_3$; 298 K): δ 0.26 (t, $^1J_{B-F}$ = 28.4 Hz, 1B, *BF*$_2$). HR-MS (APCI): Calculated for $C_{46}H_{18}BBrCuF_{12}N_6$ [(M + H)$^+$]: 1034.9976, observed: *m*/*z* 1034.9928.

Corrole-BODIPY Triads (8) and Porphyrin-BODIPY Pentad (9). **4** (50 mg, 0.1 mmol) and pentafluorobenzaldehyde (9.8 mg, 0.05 mmol) were dissolved in 10 mL of dry CH_2Cl_2 under argon. A solution of $BF_3{\cdot}OEt_2$ (0.3 equiv) was added to the reaction mixture and stirred for 1 h. Then, 22.7 mg (0.1 mmol) of DDQ dissolved in 1 mL of toluene was added, and the mixture was further stirred for 30 min. The solvent was removed under reduced pressure and subjected to column chromatography through silica gel (100−200 mesh) using chloroform/hexane (50:50, v/v) as eluent gave a trace of **8** (confirmed by mass spectroscopy, Figure S27, Supporting Information) along with major product **9**. Yield = 35%, (54 mg, 0.035 mmol), purple colored powder. ^{1}H NMR (500 MHz; $CDCl_3$; 298 K): δ −2.69 (s, 2H, NH), δ 6.73 (m, 3H, *bodipy pyrrolic*), δ 7.12 (m, 3H, *bodipy pyrrolic*), δ 7.65 (s, 2H, *bodipy pyrrolic*), δ 7.68 (s, 1H, *bodipy pyrrolic*), δ 7.72−7.74 (m, 12H, *corrole pyrrolic*), δ 8.17 (s, 3H, *bodipy pyrrolic*), δ 8.70 (s, 3H, *bodipy pyrrolic*) δ 8.78 (d, $^3J_{H-H}$ = 4.7 Hz, 2H, *corrole pyrrolic*), δ 9.15 (m, 6H, *corrole pyrrolic*). ^{19}F NMR (376 MHz; $CDCl_3$; 298 K): δ −161.84 (m, 2F, *meta Ph-F*), δ −152.29 (t, $^3J_{F-F}$ =20.9 Hz, 1F, *para Ph-F*), δ −144.54 (dd, $^1J_{F-B}$ = 56.6 Hz, $^1J_{F-B}$ = 27.8 Hz, 6F, *BF*$_2$), δ −136.78 (m, 2F, *ortho Ph-F*). ^{11}B NMR (128 MHz; $CDCl_3$; 298 K): δ 0.68 (t, $^1J_{B-F}$ = 28.2 Hz, 3B, *BF*$_2$). MS (MALDI-TOF, without matrix): Calculated for $C_{71}H_{40}B_3Br_3F_{11}N_{10}$ [(M + H)$^+$]: 1509.0935, observed: *m*/*z* 1509.336.

3. RESULTS AND DISCUSSION

3.1. Synthesis. Preparation of precursors **2**, **3**, and **4** were carried out (Scheme 1) according to reported procedure. Synthesis of **2** involved two steps in a one-pot reaction; oxidation of corresponding dipyrromethane **1** with DDQ followed by subsequent addition of triethylamine immediately followed by $BF_3{\cdot}OEt_2$ gave a good yield.[17] A drop in yield was observed with delayed addition of $BF_3{\cdot}OEt_2$, after the addition of triethylamine. Mono β-formylated BODIPY **3** was prepared according to a modified Vilsmeier−Haack procedure reported for BODIPY formylation.[18] Compound **4** was prepared by condensation of corresponding aldehyde and excess of pyrrole in the presence of TFA. Meso-β directly linked corrole-BODIPY dyad **6** and copper metalated dyad **7** were prepared for the first time (Scheme 2). We started with a Brønsted acid (TFA) catalyzed reaction of the respective aryl-aldehyde (**3**) and pentafluorophenyl-dipyrromethane (**5**) in CH_2Cl_2, and subsequent oxidation by DDQ gave **6** in low yield (16%). Multiple column chromatographic separations were performed

DOI: 10.1021/ic502919s
Inorg. Chem. 2015, 54, 4257−4267

Scheme 3. Synthesis of Compounds 8 and 9[a]

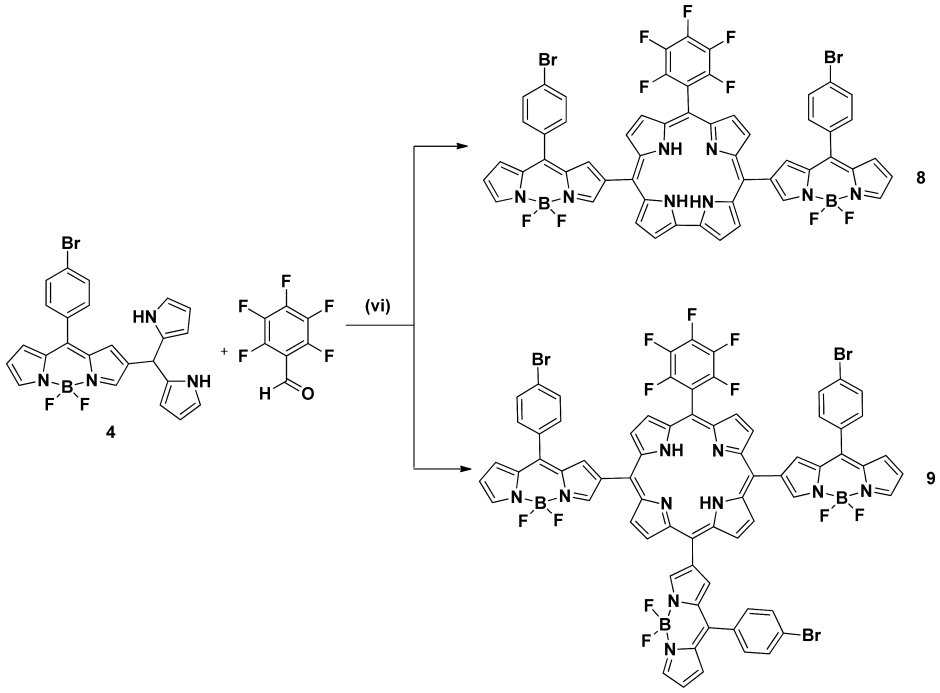

[a](vi) $BF_3{\cdot}OEt_2/CHCl_3$, DDQ, **8** (trace amount), **9** (yield = 35%).

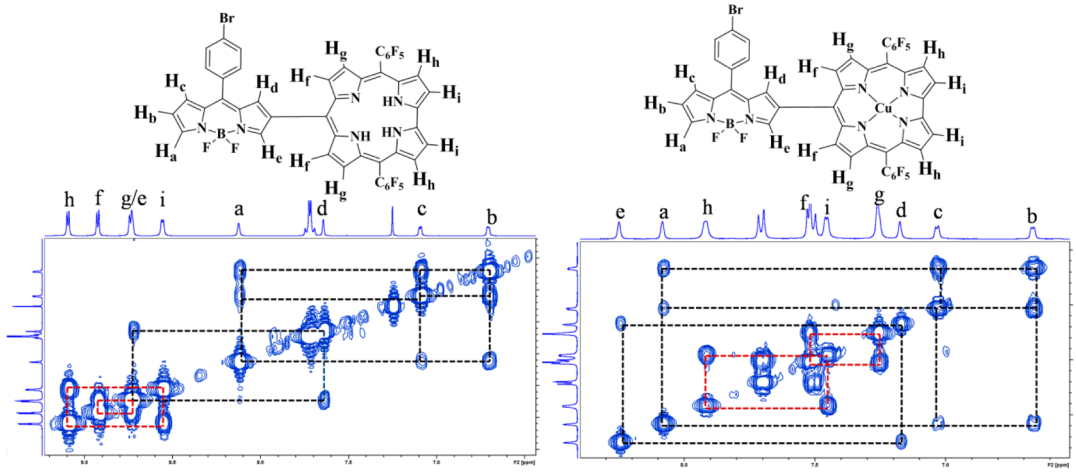

Figure 1. $^1H-^1H$ COSY spectra of compound **6** (left) and **7** (right) in $CDCl_3$ at 25 °C.

to separate overlapping bands and repeated precipitation with hexane/methanol provided pure compound. Similar separation difficulties were also observed with $BF_3{\cdot}OEt_2$ in $CHCl_3$, but with relatively improved yield (24%). Gryko and co-workers reported an excellent method for the synthesis of *meso*-arylcorrole using H_2O/MeOH (1:1, v/v) mixture as a solvent in the presence of HCl (aq) and the subsequent oxidation of bilane intermediate by DDQ/*para*-chloranil in $CHCl_3$.[19] In our case, solubility of *β*-formyl BODIPY (**3**) in MeOH was rather poor, but MeOH/H_2O (2:1, v/v) as solvent gave **6** in low yield (14%) with relatively easy separation protocol. We chose to follow a methanol–water procedure to avoid tedious separation despite lower yields. Treatment of **6** with $Cu(OAc)_2{\cdot}H_2O$ in $CHCl_3$/MeOH (1:2) afforded copper metalated compound **7** in good yield (82%).[20]

Furthermore, with an idea to attach a large number of BODIPY units directly to the meso-position of corrole, we opted for precursor **4** which reacted with pentafluorobenzaldehyde in the presence of $BF_3{\cdot}OEt_2$ in $CHCl_3$ (Scheme 3).[21] We observed only a trace amount of expected compound **8** (confirmed by mass spectroscopy, Figure S27) along with A_3B type porphyrin **9** as the major product. This unexpected formation of A_3B porphyrin was possibly an outcome of the scrambling of dipyrromethane **4**. The scrambling of dipyrromethane in acid was observed as a function of steric and electronic factor at the meso-carbon. Sterically hindered and electron-deficient substituent at the meso-carbon of dipyrromethane shows less scrambling than dipyrromethane bearing a less hindered and electron-rich group.[22]

3.2. NMR Spectra. ^1H, ^{19}F, and ^{11}B NMR spectral characterization of **6** confirmed the proposed structure. ^1H NMR spectrum exhibits characteristic sharp peaks in accordance with 17 protons in the region *δ* 6.6–9.1 ppm (Figure S17). Out of these signals four doublets (*δ* 8.55, *δ* 8.73,

DOI: 10.1021/ic502919s
Inorg. Chem. 2015, 54, 4257–4267

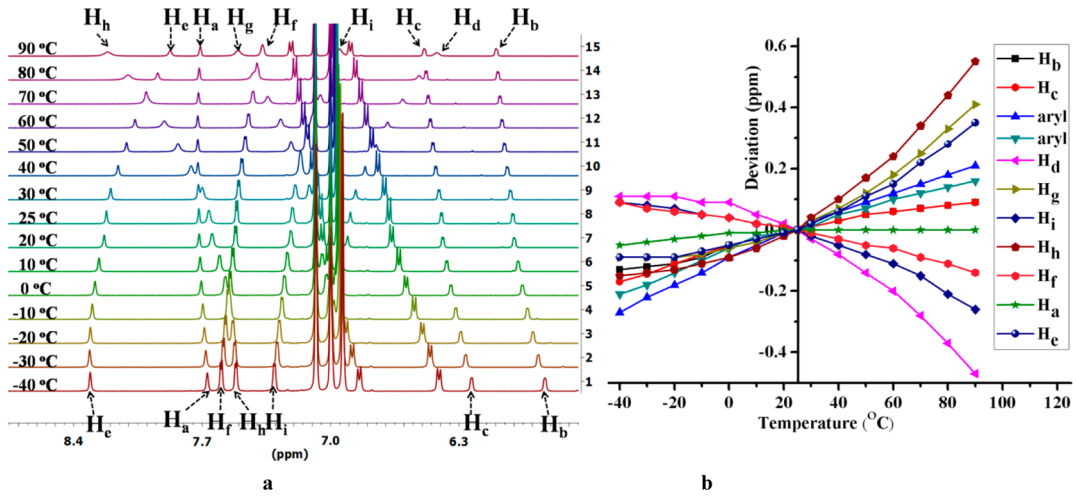

Figure 2. (a) ^{1}H NMR variable temperature experiment of **7** in toluene-d_8. (b) Plot of chemical shift deviation at different temperatures with respect to 25 °C in toluene-d_8. Positive and negative deviation corresponds to the deviation toward downfield and upfield regions with respect to 25 °C respectively.

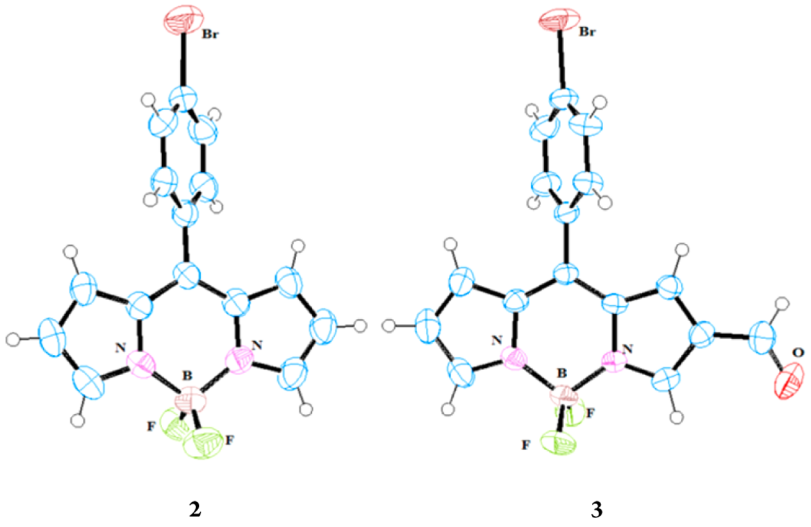

Figure 3. Single crystal structures of compounds **2** and **3** (ORTEP representations). Thermal ellipsoids at 50% probability.

δ 8.9, δ 9.08) were assigned for eight corrole β-pyrrolic protons, with a characteristic coupling constant of 4−5 Hz. Signal for the *meso*-aryl ring protons of BODIPY, two doublets with roof effect were observed at δ 7.69 and δ 7.72 ppm. Two doublets (δ 6.70, δ 7.08) with characteristic coupling constant of 3−4 Hz and three singlet (δ 7.63, δ 8.11, δ 8.72) were assigned to five BODIPY pyrrolic protons. ^{19}F NMR shows three signals (δ −136.96, δ −152.17 and δ −160.76) corresponding to two C_6F_5 (Figure S18), and a doublet of doublets at δ −144.87 ppm was assigned to BF_2. ^{11}B NMR exhibited a slightly deshielded triplet signal (δ 0.26, J = 28.4 Hz) with reference to **2** and **3** (Figures S3 and S8). In compound **7**, all proton resonances appeared slightly shielded compared to that of compound **6**. Correlation and assignment of pyrrolic protons for **6** and **7** were carried out on the basis of ^{1}H−^{1}H COSY (Figure 1), NOESY (Figures S32 and S36), ROESY (Figure S34), and HSQC (Figure S33). Black connecting lines represent a correlation among BODIPY β-pyrrolic protons, whereas red lines indicate a correlation between β-pyrrolic protons of corrole. The ^{1}H−^{1}H correlation spectrum reveals the resonance of bipyrrolic β-protons of **6**, namely, H_f and H_g flanked by the resonances of H_h and H_i. BODIPY β-pyrrolic protons H_a−H_c and H_d−H_e give relatively weak correlation due to long-range coupling in both compounds, whereas proton H_b shows a strong correlation between both H_a and H_c. ^{1}H NMR signals of corrole β-pyrrolic protons in compound **7** appear relatively broad at room temperature. To understand the effect of temperature on the chemical shift and nature of the signal, a variable temperature ^{1}H NMR experiment was conducted for compound **7** in toluene-d_8 (Figure 2). All corrole β-pyrrolic signals experience considerable shift in either direction along with simultaneous broadening at a higher temperature. This broadening of peaks can be ascribed to Cu(II)-corrole π-radical cations.[20a,23] Saddling geometry of Cu (III)-corrole imparts unique properties of temperature-dependent magnetic behaviors. Saddling induces a part of the electron density from HOMO of the corrole moiety to flow into the empty $d_{x^2-y^2}$ orbital of the Cu(III) metal center.[24] Theoretical calculation by Abhik Ghosh et al. suggested that ground state Cu(III)-corrole complex is only slightly lower in energy than Cu(II)-corrole π-radical cationic state.[25] This small energy barrier can be thermally accessible. Thus, a temperature-

DOI: 10.1021/ic502919s
Inorg. Chem. 2015, 54, 4257−4267

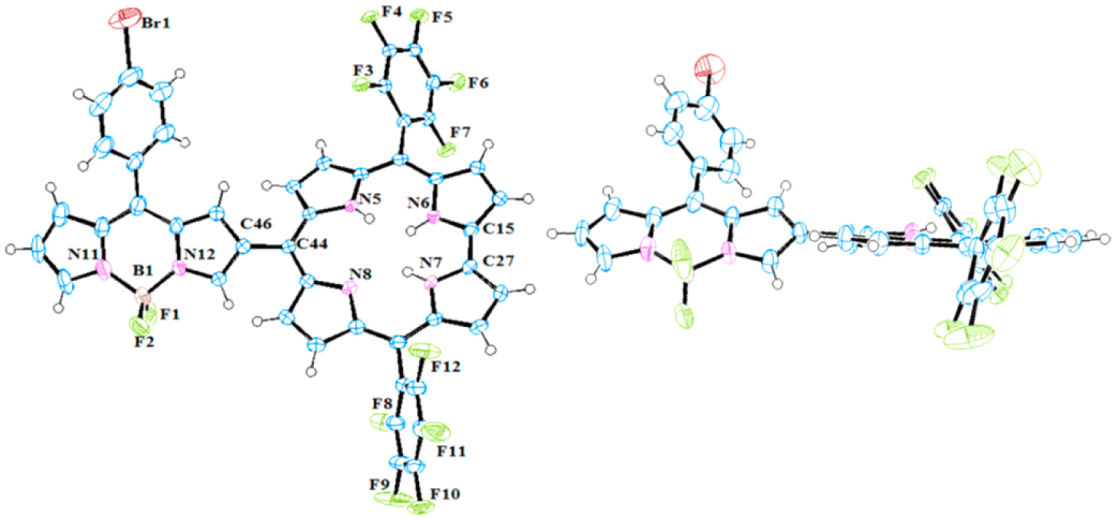

a b

Figure 4. Single crystal X-ray structures of compound **6** (ORTEP representations). (a) (side view) and (b) (view toward corrole plane). Thermal ellipsoids at 50% probability.

dependent equilibrium between diamagnetic d^8 Cu(III)-corrole and paramagnetic d^9 Cu(II)-corrole π-cation radical was strongly reflected in this copper complex. The BODIPY β-pyrrolic protons H_e and H_d directly connected to the meso-carbon of corrole are the most affected by the paramagnetism of corrole core due to close proximity and further resonate at the shielded region, while the remaining protons of BODIPY do not indicate considerable temperature-dependent behavior other than the appearance of doublet splitting pattern as the temperature increases. In the case of **6** temperature has a very weak effect except broadening of the signal with a decrease in temperature (Figure S37).

3.3. X-ray Diffraction Studies. Structures of **2**, **3**, and **6** are shown in Figures 3 and 4 respectively. Crystals suitable for X-ray diffraction analysis for **3** and **6** were grown by vapor diffusion of *n*-hexane into a dichloromethane solution at 4 °C, whereas for **2** was obtained by slow evaporation of dichloromethane solution at room temperature. The relevant crystallographic data for these compounds are summarized in Table 1. Compound **6** was crystallized in monoclinic $P21/c$ space group. Twenty-three atoms in $C_{19}N_4$ corrole core have nonplanar conformation with a small saddle distortion and are quite similar to that previously observed for free-base corrole macrocycles.[26] The mean plane deviation of its 23 atoms is 0.102 Å, with a maximum of 0.232 Å for N5. The interior N atoms in the corrole core are forced to deviate out from coplanarity, two above and two below, due to steric repulsion from three inner hydrogens. The bond distance (1.473 Å) between the meso-carbon of corrole connected to BODIPY β-pyrrolic carbon is slightly shorter than two pentafluorophenyl meso-substituents (1.482 and 1.497 Å). Mean planes of BODIPY units are rotated by about 45.41° with respect to the corrole core mean plane, while the two pentafluorophenyl rings are tilted by about 72.46° and 53.99°, respectively.

The DFT optimized geometry (Figures 5 and S38), calculated bond distances and angles, matches fairly well with the experimental values and is summarized in Table 2. In compounds **6** and **7** HOMO is mainly localized on the electron-rich corrole moiety. Notably, in **6**, LUMO is localized on the BODIPY fragment, whereas in the case of **7**, LUMO+1 is localized on the BODIPY fragment.

Table 1. Crystal Data and Structures Refinement for Complexes

	2	3	6
CCDC	1023162	1023022	1022285
formula	$C_{15}H_{10}BBrF_2N_2$	$C_{16}H_{10}BBrF_2N_2O$	$C_{46}H_{20}BBrF_{12}N_6$
M_w (g mol^{-1})	346.96	374.97	975.39
crystal system	triclinic	monoclinic	monoclinic
space group	$P\bar{1}$	$P21/c$	$P21/c$
a (Å)	7.7681(4)	11.5531(8)	15.9618(19)
b (Å)	7.9220(4)	8.7314(7)	8.356(1)
c (Å)	11.8432(6)	15.0856(10)	34.582(4)
α (deg)	85.630(3)	90	90
β (deg)	80.383(3)	97.196(3)	113.041(5)
γ (deg)	74.105(3)	90	90
V (Å^3)	690.74(6)	1509.77(19)	4244.5(9)
Z	2	4	4
D_{calcd} (g cm^{-3})	1.668	1.650	1.526
μ (mm^{-1})	2.990	2.748	1.063
F(000)	344.0	744.0	1944.0
temperature (K)	296	296	105
λ [Å]	0.71073	0.71073	0.71073
θ-range for data collection (deg)	28.690	27.980	28.010
measured reflection	3568	3635	10240
T_{min}, T_{max}	0.307, 0.460	0.307, 0.463	0.655, 0.775
R_1 [$I > 2\sigma(I)$]	0.0475(2401)	0.0445(2479)	0.0858(5561)
R_w [$I > 2\sigma(I)$]	0.1736(3469)	0.1615(3624)	0.2419(1015)
goodness-of-fit [GOF]	1.183	1.092	1.041

3.5. Redox Properties. Electrochemical properties of compounds **2**, **3**, **6**, **7** and 5,10,15-tris(pentafluorophenyl)-corrole [H_3(tpfc)] were investigated in CH_2Cl_2, and potentials with reference to Ag/Ag^+ electrode are given in Table 3. Cyclic voltammograms of **2** and **3** (Figures S39 and S40) consist of two irreversible oxidation peaks, and two reversible reduction peaks. Because of the presence of the formyl group in **3**, it is relatively difficult to oxidize and easier to reduce than **2**. The difference in the first oxidation potential and reduction potential between **2** and **3** varied by ~21 mV and ~25 mV respectively. A thorough investigation on redox behavior of

DOI: 10.1021/ic502919s
Inorg. Chem. 2015, 54, 4257−4267

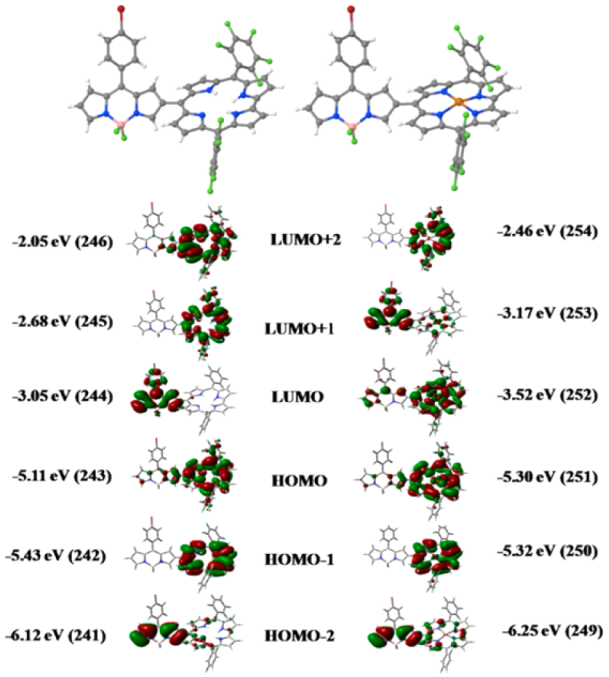

Figure 5. DFT optimized geometry and frontier orbital plots of compounds **6** (left) and **7** (right).

free-base corrole was carried out by Kadish and co-workers in nonaqueous solvent (PhCN and pyridine) and confirmed the involvement of a mixture of *in situ* generated electroactive species in the redox process due to facile gain and loss of protons.[27] Electroreduction of compound **6** (Figure 6) revealed two irreversible peaks at $E_p = -0.94$ V (BODIPY centered) and $E_p = -1.37$ (corrole centered). The initial electrooxidation of neutral species (Bod-Cor)H_3 was irreversible and located at $E_p = 0.66$ V. This led to the formation of species $[(\text{Bod-Cor})H_2]^{\bullet}$ and $[(\text{Bod-Cor})H_4]^{+}$. This mixture of electroactive species further involved two reversible oxidations at $E_{1/2} = 0.74$ V and $E_{1/2} = 0.91$ V respectively. A reversible oxidation peak at $E_{1/2} = 1.23$ V and an ill-defined oxidation peak observed during reverse scan at $E_p = 0.12$ V were assigned to a corrole fragment. A BODIPY centered oxidation process at potential 1.57 V was observed in DPV. The redox properties of 5,10,15-tris-(pentafluorophenyl)corrole [H_3(tpfc)] as reference compound in CH_2Cl_2 were also investigated (Figure S41). A similar voltammogram was observed which indicates the involvement of similar redox active species. The cyclic voltammogram of compound **7** is displayed in Figure 7 and consists of three reduction and two oxidation processes. Copper metal-centered facile one electron reversible reduction peak at $E_{1/2} = 0.02$ V was observed, which is similar to that observed for the Cu(III)-corrole complex.[16a,f−i] Ligand centered irreversible reduction and reversible oxidation were observed at $E_p = -1.29$ V and $E_{1/2} = 0.90$ V respectively, whereas irreversible oxidation and reduction peaks at $E_p = 1.59$ V and $E_p = -0.92$ V were assigned to the BODIPY unit. Redox properties of BODIPY fragments in **6** and **7** do not show any considerable difference to that observed in reference compounds **2**. This electronic isolation between the chromophoric fragments remains intact despite the shortest bond connection and probably due to the tilted orientation of the BODIPY unit with respect to the corrole fragment as observed in solid state structural studies.

3.6. UV−vis Absorption Study. Ground state absorption spectra of compounds **2**, **3**, **6**, **7**, and **H_3(tpfc)** in CH_2Cl_2 have been shown for the comparison in Figure 8. BODIPY **2** and **3** display the typical narrow absorption features with λ_{max} positioned at 503 and 498 nm, respectively.[28] This absorption band is assigned to the S_0-S_1 transition. An additional weaker and broad absorption band at ∼300−400 nm was also observed which corresponds to the S_0-S_2 transition. Absorption maximum of **3** was observed to be ∼5 nm blue-shifted to that of **2**. The observed hypsochromic shift can be rationalized due to stabilization of HOMO by the presence of an electron-withdrawing formyl group in the β-position of **3**. Compound **6** exhibits a typical corrole Soret type band around 411 nm and broad Q type bands from 500 to 750 nm. An additional absorption band corresponding to BODIPY chromophoric fragment was also observed at 488 nm. Similarly, compound **7** exhibits a Soret type band at 398 nm, Q type bands around

Table 2. Selected X-ray and DFT Calculated Bond Distances [Å] and Angles [deg] for Compound 6 and 7

	crystal structure	DFT (B3LYP) optimized geometry	
	6	**6**[6-31G (d)]	**7** [631G (d) +LANL2DZ]
Br(1)−C(91)	1.886(7)	1.907	1.905
N(11)−B(1)	1.554(9)	1.566	1.566
N(12)−B(1)	1.540(6)	1.571	1.571
B(1)−F(1)	1.357(8)	1.379	1.378
B(2)−F(2)	1.393 (7)	1.382	1.382
C(15)−C(27)	1.407(6)	1.418	1.429
C(44)−C(46)	1.473(6)	1.479	1.469
Cu−N(14)			1.924
Cu−N(15)			1.918
Cu−N(16)			1.919
Cu−N(17)			1.923
F(1)−B(1)−F(2)	111.7(5)	111.8	112.0
F(1)−B(1)−N(11)	111.5(5)	110.0	110.1
F(1)−B(1)−N(12)	110.8(5)	109.1	110.4
C(35)−C(44)−C(46)	117.5(4)	118.0	117.8
C(45)−C(44)−C(46)	115.7(4)	116.3	117.7
N(7)−C(27)−C(15)	116.1(4)	116.1	112.6
N(6)−C(15)−C(27)	114.0(4)	115.6	112.6

DOI: 10.1021/ic502919s
Inorg. Chem. 2015, 54, 4257−4267

Table 3. Half-Wave or Peak Potential (V vs Ag/Ag^+) for 2, 3, 6, 7, and H_3(tpfc) in CH_2Cl_2 Containing 0.1 M TBAP

	oxidation						reduction		
compounds	VI	V	IV	III	II	I	I	II	III
2					2.05[b]	1.59[b]	−0.80	−1.68[b]	
3					2.26[b]	1.80[b]	−0.55	−1.19[b]	
6	1.57[b]	1.23	0.91	0.74	0.66[a]	0.12[a]	−0.83[b]	−1.28[b]	
7					1.59[a]	0.90	0.02	−0.83[b]	−1.18[b]
tpfc			1.04	0.90	0.78[a]	0.22[a]	−1.24[b]		

[a]Oxidation or reduction peak potential. [b]DPV oxidation or reduction potential.

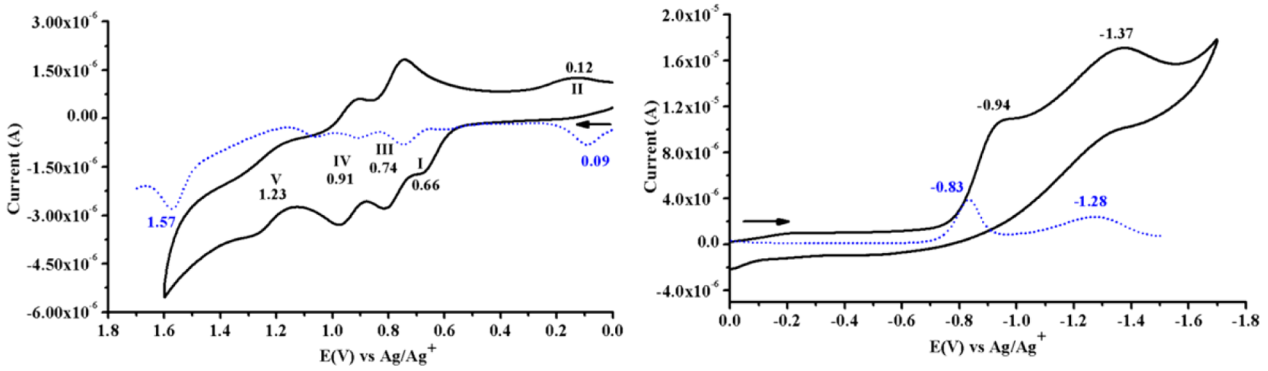

Figure 6. Cyclic voltammogram (solid line) at scan rate: 0.1 V/s and differential pulse voltammogram (dotted line) of **6** in CH_2Cl_2.

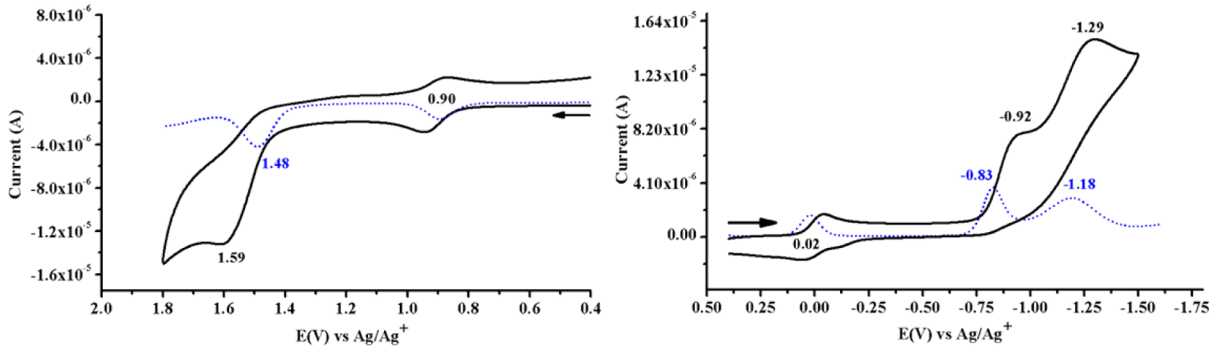

Figure 7. Cyclic voltammogram (solid line) at scan rate: 0.1 V/s and differential pulse voltammogram (dotted line) of **7** in CH_2Cl_2.

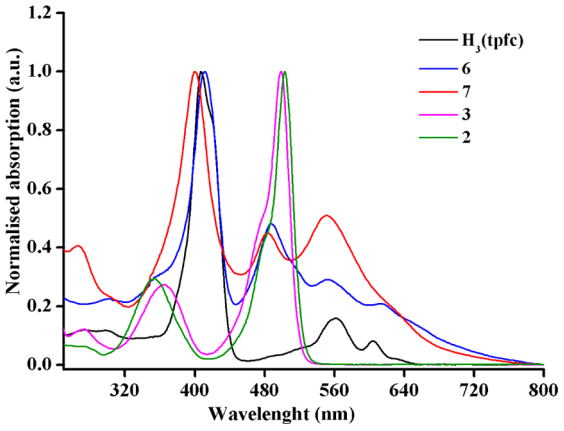

Figure 8. UV−vis absorption spectra of compound **H_3(tpfc)** (black), **6** (blue), **7** (red), **3** (pink), and **2** (green) in CH_2Cl_2.

500−750 nm, and an additional absorption band contribution from the BODIPY fragment at 484 nm. Both choromophoric fragments in dyads **6** and **7** exhibit an overall additive absorption spectrum spanning throughout the UV−vis region of 250−750 nm. Furthermore, absorption spectra support weak ground state electronic communication between chromophores as indicated in cyclic voltammetric studies.

3.7. Protonation and Deprotonation Study. The protonation study of **6** was carried out with the addition of trifluoroacetic acid (TFA) in CH_2Cl_2 solution. Addition of TFA produced a color change from purple to brown as shown in Figure 11. UV−vis absorption spectrum shows diminishing bands at 411 and 489 nm with concomitant enhancement of bands at 474, 556, and 645 nm. The Job's plot analysis revealed a 1:1 stoichiometry of complexation between H^+ and **6** (Figure S46). With the help of a straight line from $[TFA]^2/A_0\text{-}A_n$ versus $[TFA]^2$, the equilibrium constant log K was calculated to be 5.08 (Figure 9). Notably, protonation by TFA induced band at 489 nm, corresponding to BODIPY absorption to be blue-shifted by 15 nm. Monoprotonation of inner nitrogen increases positive charge density on corrole moiety. Thus, probably the corrole moiety stabilized the HOMO of BODIPY due to increase in electronegativity, which then resulted in a blue-shifted band.

Solid state structure and DFT optimized geometry in **6** revealed that the NH-protons suffered severe steric hindrance

DOI: 10.1021/ic502919s
Inorg. Chem. 2015, 54, 4257−4267

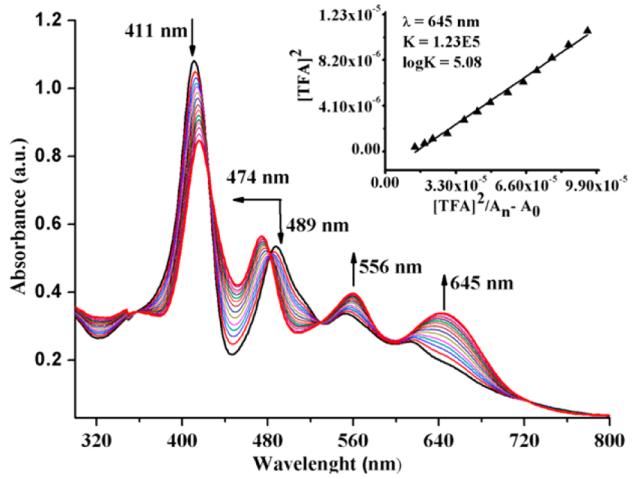

Figure 9. UV−vis absorption change of **6** (~10^{-6} M) with the addition of TFA in CH_2Cl_2 solution.

which causes interior protonated nitrogen to deviate out of the mean pyrrole ring plane. This out-of-plane deviation to minimize steric repulsion accounts for the observed higher acidity for corrole macrocycles.[29] To understand the deprotonation behavior, a non-nucleophilic base 1,8-diazabicyclo[5.4.0]undec-7-ene (DBU) was added to **6** in CH_2Cl_2. This resulted in an immediate color change of the solution from purple to green (Figure 11). UV−vis absorption changes were monitored with the addition of increasing amount of DBU in CH_2Cl_2 solution (Figure 10). An

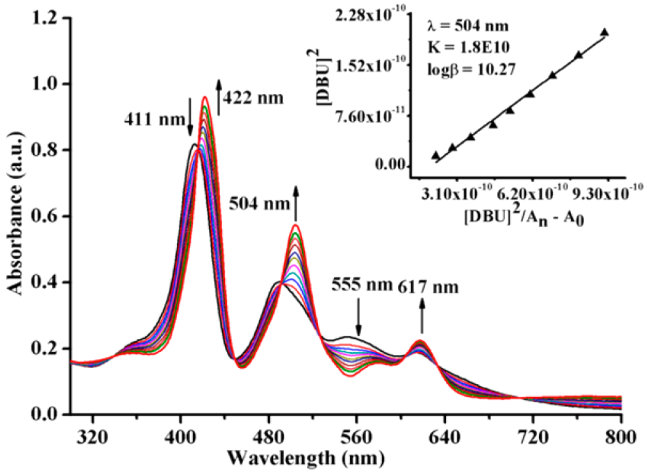

Figure 10. UV−vis absorption change of **6** (~10^{-6} M) with the addition of DBU in CH_2Cl_2 solution.

enhancement of bands at 422 nm, 504 nm, 617 nm with simultaneous diminishing bands at 411 and 550 nm was observed. The Job's plot referred to a 1:1 stoichiometric interaction between **6** and DBU (Figure S45). With the help of sa traight line plot from $[DBU]^2/A_n$-A_0 versus $[DBU]^2$, the equilibrium constant log β was found to be 10.27. Encouraged from the DBU deprotonation study, we opted to explore easy deprotonation behavior of **6** toward the sensing ability of various anions. We studied various common anions (F^-, Cl^-, Br^-, I^-, CH_3COO^-, $H_2PO_4^-$, HSO_4^-, and NO_3^-) in the form of TBA salt in a CH_2Cl_2 solution. Addition of highly basic anions F^-, AcO^-, and $H_2PO_4^-$ shows immediate colorimetric changes from brown to green color (Figure 11), while the rest of tested anions do not produce any effect even with 50 fold

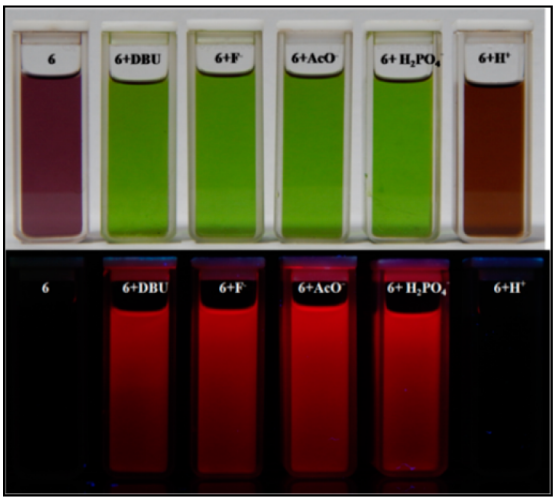

Figure 11. Colorimetric change of **6**, above under daylight and below under UV light. Picture was taken with 10 equiv additions of DBU, F^-, AcO^-, $H_2PO_4^-$, and TFA in CH_2Cl_2 solution of **6** (~10^{-4} M).

addition. Upon higher addition of F^- (Figures S43 and S44 for AcO^- and $H_2PO_4^-$ respectively), an intense band emerged at 426 nm, 507 nm, 621 nm with simultaneous disappearance of bands at 411 and 560 nm as shown in Figure 12. The Job's plot

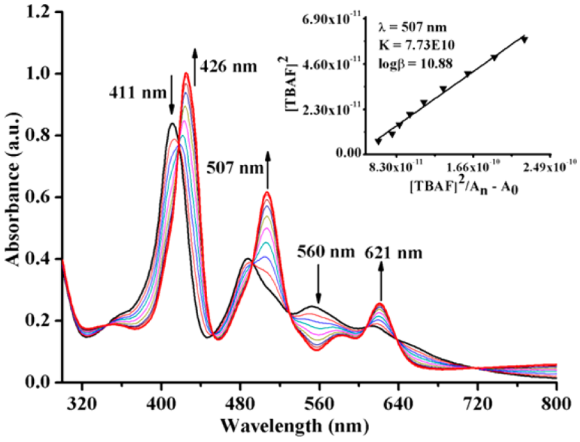

Figure 12. UV−vis absorption change of **6** (~10^{-6} M) with the addition of TBAF in CH_2Cl_2 solution.

referred to 1:2 stoichiometric interactions of **6** with all interacting basic anions (Figure S47). The visible color and UV−vis absorption changes with F^-, AcO^-, and $H_2PO_4^-$ were similar to that as observed in the case of DBU addition. These results support the fact that the spectral and colorimetric changes were possibly due to deprotonation of NH moiety of corrole by basic anions. Furthermore, the initial band at 488 nm which corresponds to absorption of BODIPY fragment was red-shifted by 18 nm to a new band at 507 nm with the addition of F^-. An ^1H NMR study with F^- addition shows the appearance of new peaks in the shielded region as shown in Figure 13. These shielded proton signals strongly support increased electron density due to deprotonation of the inner NH proton of corrole.

DOI: 10.1021/ic502919s
Inorg. Chem. 2015, 54, 4257−4267

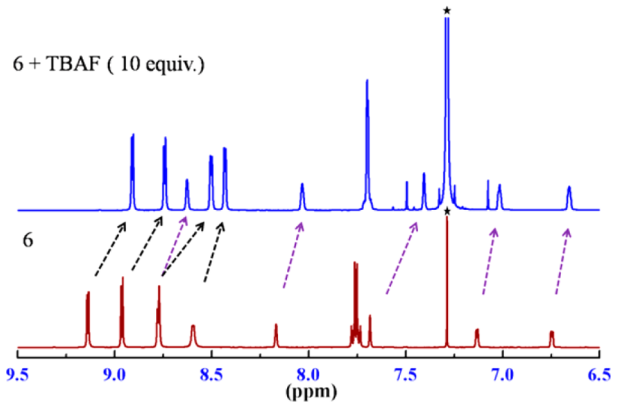

Figure 13. Partial ^{1}H NMR of **6** with an addition of TBAF in $CDCl_3$. Black arrows (corrole) and purple arrows (BODIPY) represent a shift of corresponding protons.

Furthermore, quite interestingly, we observed a pink color fluorescence "turn on" phenomenon with the addition of basic anions (DBU, F^-, AcO^-, and $H_2PO_4^-$) as shown in Figure 11. Addition of F^- in CH_2Cl_2 solution shows a gradual enhancement of an emission band at 665 nm, which is a typical corrole based emission (Figure 14). Compound **6** was initially

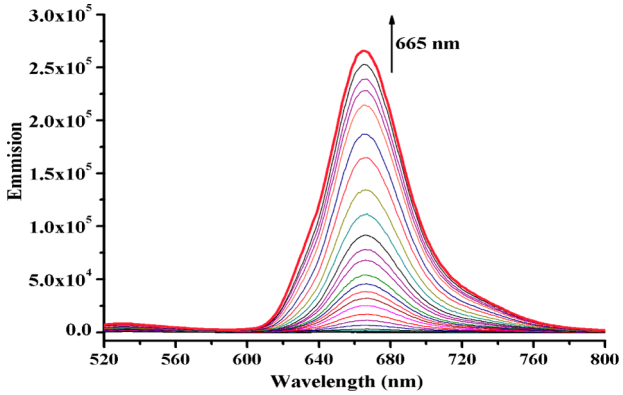

Figure 14. Fluorescence enhancement of **6** ($\sim 10^{-5}$ M) with the addition of TBAF in CH_2Cl_2 solution. Excitation at λ = 411 nm.

nonfluorescent, probably because of excited state electron transfer between the corrole and BODIPY unit, which is one of the fundamental quenching phenomena for chromophoric donor–acceptor (D–A) types of molecules as commonly observed for many similar systems.[13,30] A negative free energy change (ΔG_{CS} = −0.78 eV) suggests a thermodynamically feasible photoinduced electron transfer (PET) event from singlet excited state of corrole to the BODIPY, yielding a charge separated state (Figure S42). It was observed that deprotonation of NH enhanced the emission quantum yield of corrole but does not have much effect in the fluorescence lifetime of corrole anion.[31] Fluorescence lifetime of deprotonated species of **6** in CH_2Cl_2 was found to be 3.6 ns, which is close to that measured for neutral H_3(tpfc) (4.9 ns) and H_3(tpfc) anion (5.2 ns) in CH_2Cl_2 (Figure S48). Thus, the turn on fluorescence in this particular case is not because of modulation or quenching of any electron transfer process present, but merely an outcome of higher fluorescence quantum yield of corrole-anion. This observation was quite different from reported fluorescence "turn on" phenomenon where quenching of the electron or energy transfer process mostly restores the fluorescence.[32] We observed a fine balance between complete fluorescence quenching of neutral corrole molecule probably due to electron transfer and afterward gradual enhancement of emission solely due to the inherent higher emission behavior of corrole-anion. Experimental equilibrium constant (log β) for F^- was found to be 10.88, which is close to that of DBU, whereas AcO^- and $H_2PO_4^-$ have a relatively small log β value of 8.99 and 8.27 respectively (Figures S37 and S38). A higher equilibrium constant of F^- can be attributed to higher electronegativity (4.1) and smaller size (1.3 Å). Moreover the size of fluoride ion is compatible with the smaller corrole core size of 2.5 Å.

3.9. Conclusion. We have presented here the synthesis of the bichromophoric meso-β linked free-base corrole-BODIPY dyad **6** and its Cu (III)-metalated derivative **7**. Single crystal X-ray structure of **6** revealed a saddle distortion of corrole core with two nitrogen atoms alternatively in an up and down conformation. Distortion of corrole core relieved the steric hindrance experienced by the three inner nitrogen protons and resulted in a higher acidic nature. A tilted orientation by about 45.41° was observed between corrole and BODIPY. ^{1}H NMR of compound **7** exhibits strong temperature-dependent resonance with broadening and shifting of signals due to paramagnetic contribution of Cu(II)-corrole π-radical cation. CV and UV–vis studies suggested weak ground state electronic communication between the chromophoric fragments.

Similar to the case of a singly connected porphyrin-BODIPY dyads, emission was quenched due to a possible electron transfer process. However, it is demonstrated here that the fluorescence can be revoked by the addition of either a neutral base or suitable anion like F^-. Thus, the current study displays the uniqueness of the corrole-BODIPY dyad which is unlike that of the porphyrin BODIPY unit.

■ ASSOCIATED CONTENT

Ⓢ Supporting Information

NMR spectra, mass spectra, UV–vis spectra, CV plot, TCSPC, and DFT optimized geometry. This material is available free of charge via the Internet at http://pubs.acs.org.

■ AUTHOR INFORMATION

Corresponding Author

*E-mail: sankar@iiserb.ac.in. Fax: +91-755-6692392. Tel: +91-755-6692-334.

Notes

The authors declare no competing financial interest.

■ ACKNOWLEDGMENTS

B.B. acknowledges UGC for JRF fellowship. A.R.S and R.R. thank IISER, Bhopal for a fellowship. J.S. thanks DST, New Delhi, MHRD, New Delhi, and IISERB for funding.

■ REFERENCES

(1) Johnson, A. W.; Kay, I. T. *J. Chem. Soc.* **1965**, 1620–1629.
(2) Gross, Z.; Galili, N.; Saltsman, I. *Angew. Chem., Int. Ed.* **1999**, *38*, 1427–1429.
(3) Paolesse, R.; Jaquinod, L.; Nurco, D. J.; Mini, S.; Sagone, F.; Boschi, T.; Smith, K. M. *Chem. Commun.* **1999**, 1307–1308.
(4) Gryko, D. T. *Chem. Commun.* **2000**, 2243–2244.
(5) Brinas, R. P.; Brückner, C. *Synlett* **2001**, *3*, 442–444.
(6) Collman, J. P.; Decreau, R. A. *Tetrahedron Lett.* **2003**, *44*, 1207–1210.
(7) Flamignia, L.; Gryko, D. T. *Chem. Soc. Rev.* **2009**, *38*, 1635–1646.

DOI: 10.1021/ic502919s
Inorg. Chem. 2015, 54, 4257–4267

(8) (a) Broring, M.; Brgeier, F.; Tejero, E. C.; Hell, C.; Holthausen, M. C. *Angew. Chem., Int. Ed.* **2007**, *46*, 445−448. (b) Stefanelli, M.; Nardis, S.; Tortora, L.; Fronczek, F. R.; Smith, K. M.; Licocciaa, S.; Paolesse, R. *Chem. Commun.* **2011**, *47*, 4255−4257. (c) Steene, E.; Wondimagegn, T.; Ghosh, A. *J. Phys. Chem. B* **2001**, *105*, 11406−11413. (d) Zakharieva, O.; Schünemann, V.; Gerdan, M.; Licoccia, S.; Cai, S.; Walker, F. A.; Trautwein, A. X. *J. Am. Chem. Soc.* **2002**, *124*, 6636−6648.

(9) (a) Dogutan, D. K.; Mcguire, R., Jr.; Nocera, D. G. *J. Am. Chem. Soc.* **2011**, *133*, 9178−9180. (b) Mahammed, A.; Gross, Z. *J. Am. Chem. Soc.* **2005**, *127*, 2883−2887. (c) Gross, Z.; Gray, H. B. *Adv. Synth. Catal.* **2004**, *346*, 165−170. (d) Gross, Z.; Simkhovich, L.; Galili, N. *Chem. Commun.* **1999**, 599−600. (e) Harischandra, D. N.; Lowery, G.; Zhang, R.; Newcomb, M. *Org. Lett.* **2009**, *11*, 2089−2092.

(10) Aviva, I.; Gross, Z. *Chem. Commun.* **2007**, 1987−1999.

(11) (a) Collman, J. P.; Kaplun, M.; Decreau, R. A. *Dalton Trans.* **2006**, 554−559. (b) Kadish, K. M.; Frémond, L.; Ou, Z.; Shao, J.; Shi, C.; Anson, F. C.; Burdet, F.; Gros, C. P.; Barbe, J.-M.; Guilard, R. *J. Am. Chem. Soc.* **2005**, *127*, 5625−5631. (c) Kadish, K. M.; Frémond, L.; Shen, J.; Chen, P.; Ohkubo, K.; Fukuzumi, S.; Ojaimi, O. E.; Gros, C. P.; Barbe, J.-M.; Guilard, R. *Inorg. Chem.* **2009**, *48*, 2571−2582.

(12) (a) Barbe, J. M.; Canard, G.; Brandès, S.; Jérôme, F.; Dubois, F.; Guilard, R. *Dalton Trans.* **2004**, 1208−1214. (b) Barbe, J. M.; Canard, G.; Brandes, S.; Guilard, R. *Angew. Chem., Int. Ed.* **2005**, *44*, 3103−3106. (c) Kurzatkowska, K.; Dolusic, D.; Dehaen, W.; Stoltny, K. S.; Sieron, A.; Radecka, H. *Anal. Chem.* **2009**, *8*, 7397−7405. (d) Pariyar, A.; Bose, S.; Chhetri, S. S.; Biswasb, A. N.; Bandyopadhyay, P. *Dalton Trans.* **2012**, *41*, 3826−3831. (e) Santos, C. I. M.; Oliveira, E.; Barata, J. F. B.; Faustino, M. A. F.; Cavaleiro, J. A. S.; Neves, M. G. P. M. S.; Lodeiro, C. *J. Mater. Chem.* **2012**, *22*, 13811−13819.

(13) (a) Brizet, B.; Desbois, N.; Bonnot, A.; Langlois, A.; Dubois, A.; Barbe, J. M.; Gros, C. P.; Goze, C.; Denat, F.; Harvey, P. D. *Inorg. Chem.* **2014**, *53*, 3392−3403. (b) Tasior, M.; Gryko, D. T.; Cembor, M.; Jaworski, J. S.; Venturac, B.; Flamigni, L. *New J. Chem.* **2007**, *31*, 247−259. (c) D'Souza, F.; Chitta, R.; Ohkubo, K.; Tasior, M.; Subbaiyan, N. K.; Zandler, M. E.; Rogacki, M. K.; Gryko, D. T.; Fukuzumi, S. *J. Am. Chem. Soc.* **2008**, *130*, 14263−14272. (d) Tasior, M.; Gryko, D. T.; Shen, J.; Kadish, K. M.; Becherer, T.; Langhals, H.; Ventura, B.; Flamigni, L. *J. Phys. Chem. C* **2008**, *112*, 19699−19709. (f) Xu, H.-J.; Bonnot, A.; Karsenti, P.-L.; Langlois, A.; Abdelhameed, M.; Barbe, J.-M.; Gros, C. P.; Harvey, P. D. *Dalton Trans.* **2014**, *43*, 8219−8229. (g) Brizet, B.; Eggenspiller, A.; Gros, C. P.; Barbe, J.-M.; Goze, C.; Denat, F.; Harvey, P. D. *J. Org. Chem.* **2012**, *77*, 3646−3650. (h) Brizet, B.; Desbois, N.; Bonnot, A.; Langlois, A.; Dubois, A.; Barbe, J.-M.; Gros, C. P.; Goze, C.; Denat, F.; Harvey, P. D. *Inorg. Chem.* **2014**, *53*, 3392−3403. (i) Gros, C. P.; Brisach, F.; Meristoudi, A.; Espinosa, E.; Guilard, R.; Harvey, P. D. *Inorg. Chem.* **2007**, *46*, 125−135.

(14) (a) Aviezer, D.; Cotton, S.; David, M.; Segev, A.; Khaselev, N.; Galili, N.; Gross, Z.; Yayon, A. *Cancer Res.* **2000**, *60*, 2973. (b) Mahammed, A.; Gray, H. B.; Weaver, J. J.; Sorasaenee, K.; Gross, Z. *Bioconjugate Chem.* **2004**, *15*, 738−746.

(15) Barata, J. F. B.; Neves, M. G. P. M. S.; Tome, A. C.; Faustino, M. A. F.; Silva, A. M. S.; Cavaleiro, J. A. S. *Tetrahedron Lett.* **2010**, *51*, 1537−1540.

(16) (a) Vestfrid, J.; Botoshansky, M.; Palmer, J. H.; Durrell, A. C.; Gray, H. B.; Gross, Z. *J. Am. Chem. Soc.* **2002**, *124*, 7411−7420. (b) Stefanelli, M.; Nardis, S.; Tortora, L.; Fronczek, F. R.; Smith, K. M.; Licoccia, S.; Paolesse, R. *Chem. Commun.* **2011**, *47*, 4255−4257. (c) Nardis, S.; Mandoj, F.; Paolesse, R.; Fronczek, F. R.; Smith, K. M.; Prodi, L.; Montalti, M.; Battistin, G. *Eur. J. Inorg. Chem.* **2007**, 2345−2352. (d) Mahammed, A.; Goldberg, I.; Gross, Z. *Org. Lett.* **2001**, *3*, 3443−3446. (e) Vestfrid, J.; Botoshansky, M.; Palmer, J. H.; Durrell, A. C.; Gray, H. B.; Gross, Z. *J. Am. Chem. Soc.* **2011**, *133*, 12899−12901. (f) Gros, C. P.; Barbe, J.-M.; Espinosa, E.; Guilard, R. *Angew. Chem., Int. Ed.* **2006**, *45*, 5642−5645. (g) Guilard, R.; Gros, C. P.; Barbe, J.-M.; Espinosa, E.; Jérôme, F.; Tabard, A. *Inorg. Chem.* **2004**, 7441−7455. (h) Pomarico, G.; Nardis, S.; Stefanelli, M.; Cicero, D. O.; Vicente, M. G. H.; Fang, Y.; Chen, P.; Kadish, K. M.; Paolesse, R. *Inorg. Chem.* **2013**, *52*, 8834−8844. (i) Berg, S.; Thomas, K. E.; Beavers, C. M.; Ghosh, A. *Inorg. Chem.* **2012**, *51*, 9911−9916. (j) Stefanelli, M.; Mandoj, F.; Mastroianni, M.; Nardis, S.; Mohite, P.; Fronczek, F. R.; Smith, K. M.; Kadish, K. M.; Xiao, X.; Ou, Z.; Chen, P.; Paolesse, R. *Inorg. Chem.* **2011**, *50*, 8281−8292. (k) Lemon, C. M.; Brothers, P. J. *J. Porphyrins Phthalocyanines* **2011**, *15*, 809−834.

(17) (a) Lazarides, T.; McCormick, T. M.; Wilson, K. C.; Lee, S.; McCamant, D. W.; Eisenberg, R. *J. Am. Chem. Soc.* **2011**, *133*, 350−364. (b) Madhu, S.; Sharma, D. K.; Basu, S. K.; Jadhav, S.; Chowdhury, A.; Ravikanth, A. *Inorg. Chem.* **2013**, *52*, 11136−11145.

(18) Yu, C.; Jiao, L.; Yin, H.; Zhou, J.; Pang, W.; Wu, Y.; Wang, Z.; Yang, G.; Hao, E. *Eur. J. Org. Chem.* **2011**, 5460−5468.

(19) Koszarna, B.; Gryko, D. T. *J. Org. Chem.* **2006**, *71*, 3707−3717.

(20) (a) Bruckner, C.; Brinas, R. P.; Baue, J. A. K. *Inorg. Chem.* **2003**, *42*, 4495−4497. (b) Ngo, T. H.; Rossom, W. V.; Dehaen, W.; Maes, W. *Org. Biomol. Chem.* **2009**, *7*, 439−444.

(21) Geier, G. R.; Ciringh, Y.; Li, F.; Haynes, D. M.; Lindsey, J. S. *Org. Lett.* **2000**, *2*, 1745−1748.

(22) (a) Littler, B. J.; Ciringh, Y.; Lindsey, J. S. *J. Org. Chem.* **1999**, *64*, 2864−2872. (b) Geier, G. R.; Littler, B. J.; Lindsey, J. S. *J. Chem. Soc. Perkin Trans. 2* **2001**, 701−711. (c) Auger, A.; Muller, A.; Swarts, J. C. *Dalton Trans.* **2007**, 3623−3633. (d) Gryko, D. T.; Jadach, K. *J. Org. Chem.* **2001**, *66*, 4267−4275. (e) Gryko, D. T. *Synthesis* **2004**, 2205−2209.

(23) (a) Will, S.; Lex, J.; Vogel, E.; Schmickler, H.; Gisselbrecht, J. P.; Haubtmann, C.; Bernard, M.; Gross, M. *Angew. Chem., Int. Ed.* **1997**, *36*, 357−360. (b) Luobeznova, I.; Simkhovich, L.; Goldberg, I.; Gross, Z. *Eur. J. Inorg. Chem.* **2004**, 1724−1732.

(24) (a) Wasbotten, I. H.; Wondimagegn, T.; Ghosh, A. *J. Am. Chem. Soc.* **2002**, *124*, 8104−8116. (b) Thomas, K. E.; Wasbotten, I. H.; Ghosh, A. *Inorg. Chem.* **2008**, *47*, 10469−10478. (c) Alemayehu, A. B.; Gonzalez, E.; Hansen, L. K.; Ghosh, A. *Inorg. Chem.* **2009**, *48*, 7794−7799.

(25) Ghosh, A.; Wondimagegn, T.; Parusel, A. B. J. *J. Am. Chem. Soc.* **2000**, *122*, 5100−5104.

(26) Stefanelli, M.; Pomarico, G.; Tortora, L.; Nardis, S.; Fronczek, F. R.; McCandless, G. T.; Smith, K. M.; Manowong, M.; Fang, Y.; Chen, P.; Kadish, K. M.; Rosa, A.; Ricciardi, G.; Paolesse, R. *Inorg. Chem.* **2012**, *51*, 6928−6942.

(27) Shen, J.; Shao, J.; Ou, Z.; Wenbo, E.; Koszarna, B.; Gryko, D. T.; Kadish, K. M. *Inorg. Chem.* **2006**, *45*, 2251−2265.

(28) (a) Qin, W.; Baruah, M.; Auweraer, M. V. D.; Schryver, F. C. D.; Boens, N. *J. Phys. Chem. A* **2005**, *109*, 7371−7384. (b) Ulrich, G.; Ziessel, R.; Harriman, A. *Angew. Chem., Int. Ed.* **2008**, *47*, 1184−120.

(29) (a) Gross, Z.; Galili, N.; Simkhovich, L.; Saltsman, I.; Botoshansky, M.; Blaser, D.; Boese, R.; Goldberg, I. *Org. Lett.* **1999**, *1*, 599−602.

(30) (a) Tasior, M.; Gryko, D. T.; Shen, J.; Kadish, K. M.; Becherer, T.; Langhals, H.; Ventura, B.; Flamigni, L. *J. Phys. Chem. C* **2008**, *112*, 19699−19709. (b) Kumar, S.; Ravikanth, M. *RSC Adv.* **2014**, *4*, 64204−64213.

(31) (a) Ding, T.; Aleman, E. A.; Modarelli, D. A.; Ziegler, C. J. *J. Phys. Chem. A* **2005**, *109*, 7411−7417. (b) Harel, I. A.; Gross, Z. *Chem.—Eur. J.* **2009**, *15*, 8382−8394. (c) Mahammed, A.; Weaver, J. J.; Gray, H. B.; Abdelasand, M.; Gross, Z. *Tetrahedron Lett.* **2003**, *44*, 2077−2079.

(32) (a) Kumar, P. A.; Ramakrishnan, V. T.; Ramamurthy, P. *J. Phys. Chem. A* **2011**, *115*, 14292−14299. (b) Qi, X.; Jun, E. J.; Xu, L.; Kim, S. J.; Hong, J. S. J.; Yoon, Y. J.; Yoonj, J. *J. Org. Chem.* **2006**, *71*, 2881−2884. (c) Bozdemir, O. L.; Guliyev, R.; Buyukcakir, O.; Selcuk, S.; Kolemen, S.; Gulseren, G.; Nalbantoglu, T.; Boyaci, H.; Akkaya, E. U. *J. Am. Chem. Soc.* **2010**, *9*, 8029−8036.

DOI: 10.1021/ic502919s
Inorg. Chem. 2015, 54, 4257−4267